JACS Au
AN OPEN ACCESS JOURNAL OF THE AMERICAN CHEMICAL SOCIETY

pubs.acs.org/jacsau
Article

Stretchable Tb−Tb Distance Regulates the Piezofluorochromic Behavior of Chiral Tb(III)-MOF upon Compression

Ziyou Zhang,[#] Dongping Deng,[#] Xiaoqian Xu,[#] Jiangwei Zhang,* Shuai Yan, Zhiying Guo, Hongliang Dong, Zhiqiang Chen,* and Zhi Su*

Cite This: *JACS Au* 2024, 4, 2050−2057

Read Online

ACCESS | Metrics & More | Article Recommendations | Supporting Information

ABSTRACT: Luminescent chiral **Tb-MOF** microcrystals with the $Tb_2(COO)_4$ subunit indicated strong green mechano-luminescence under compression. Furthermore, piezofluorochromic behavior in the diamond anvil cell was observed, with the intensity tendency of decreasing−increasing−decreasing and a shortened lifetime upon compression, due to the reversible stretchable Tb−Tb interactions. The Tb−Tb distance upon compression was refined through *in* situ high-pressure X-ray absorption spectra, which was consistent with the tendency of the piezofluorochromic intensity. *In situ* high-pressure UV−vis absorption spectra, Fourier transform infrared spectra, and powder X-ray diffraction demonstrated the full recovery of **Tb-MOF** after over 10 GPa compressions due to the semiflexible ligand. This work not only provided an ultrastable **Tb-MOF** but also illustrated the relationship of the piezofluorochromic behavior with the detailed structural transformation for the first time.

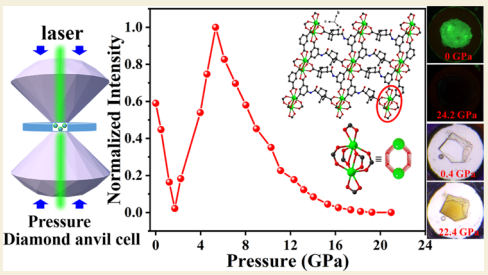

KEYWORDS: *RE-MOFs, mechano-luminescence, piezofluorochromic, high-pressure fluorescence, high-pressure XAS*

INTRODUCTION

Stimuli-responsive luminescent metal−organic frameworks (MOFs) are emerging materials, with luminescence dependent on external stimuli, such as light, heat, pressure, *etc.*[1−4] Piezofluorochromic MOFs are those structures that exhibit photophysical changes in response to external stress and may be applied in the fields of mechanical sensing, security paper, *etc.*[5−8] Traditional piezofluorochromic materials including organic and organometallic materials are observed with the ball-milling treatment, and they tend to lose both crystallinity and fluorescence once high pressure is applied (GPa scale). Detailed information on the structural transformation upon compression, however, has rarely been illustrated, and it is a great challenge to reveal the subtle relationship between the piezofluorochromic performance and the structural information.[9,10] To simplify the issue, luminescent rare-earth MOFs (RE-MOFs) were first considered due to their characteristic fluorescence, which related solely to the constituent RE ions.[11,12] Upon compression, RE-MOFs indicated no wavelength shift.

On the other hand, semiflexible ligands would be great candidates to build mechanically stable MOF.[13−16] According to our previous studies, MOFs with rigid ligands easily collapse under high pressure. For example, the irreversible breakage of Zr−O(carboxylate) coordination bonds was observed in rigid UiO-66 up to 0.4 GPa compression.[17] The μ_2-η_1:η_1 bridging carboxylate group in the rigid oriented $Zr_6O_4(OH)_4(COO)_{12}$ subunit undergoes a change in coordination to the μ_1-η_1:η_0 monodentate carboxylate group. However, the MOFs based on flexible ligands commonly underwent interpenetration and they did not collapse.[18,19] The flexible ligand is characterized by a stretchable backbone upon compression. For example, isostructural UiO-67 and UiO-abdc, with the same connected metal cluster, were built with the ligands 4,4′-biphenyldicarboxylate and 4,4′-azobenzenedicarboxylate, respectively. With the addition of the flexible diazo linker, the mechanical stability of UiO-abdc could reach up to 1.8 GPa, while UiO-67 could only maintain up to 0.3 GPa.[20] Moreover, both UiO-66 and UiO-67 underwent structural transformation at low pressure, indicating that the extended ligand could not strengthen the mechanical stability of MOFs.

Currently, MOF materials have indicated superior performance in the laboratory as a gas separator and a catalyst; however, their industrial applications are very limited. This is mainly due to the unknown mechanical property.[15] Materials with extensive ductility and bendability would be beneficial for their industrial processing, which is highly dependent on mechanical stability.[21] In fact, research on the mechanical properties of MOF materials under the high-pressure condition is still in the early stages.[22] The relationship between MOF structure and mechanical performance remains unclear.[13−15]

Received: March 20, 2024
Revised: May 1, 2024
Accepted: May 1, 2024
Published: May 11, 2024

Therefore, developing mechanical ultrastable MOFs is significant to promote their industrial applications.

Moreover, MOF materials crystallizing in piezoelectric space groups should generate mechano-luminescence (ML) due to surface cracking under external stress. Such cracked surfaces should be immediately electrified to form positive and negative charges, respectively, and the subsequent discharge process would activate the excited states. The structure should then decay to the ground state *via* emitting ML.[23−28] This would ensure the successful observation of the piezofluorochromic phenomenon upon compression. Thus, the presence of a chiral ligand with no symmetric centers would enhance the potential for MOF to crystallize in the piezoelectric space groups. Once the chiral ligand coordinated to metal ions or clusters, the resulting MOF materials with a dipole structure or non-centrosymmetric arrangement would achieve the piezoelectric property and facilitate the generation of ML under compression.[29−32] Thus, a chiral semiflexible RE-MOF crystallizing in a piezoelectric space group would be the potential candidate to build a connection between structure and piezofluorochromic performance upon compression.

Inspired by these analyses, a chiral semiflexible ligand H_3(*CAM*−*MBA*), named 5-((3*s*)-3-carboxy-2,2,3-trimethylcyclopentane-1-carboxamido)isophthalic acid, was first synthesized from the chiral flexible camphoric acid and the rigid 5-aminom-phthalic acid (Figure 1, Experimental Section). **Tb-MOF**, **Yb-MOF**, and bimetallic (**Tb_xYb_{2-x}**)**-MOF** were obtained (Experimental Section). Investigations demonstrated that **Tb-MOF** exhibits a strong green ML and piezofluorochromic performance, ascribed to the reversible stretching of the Tb−Tb interaction. *In situ* high-pressure studies revealed that **Tb-MOF** maintains high crystallinity after compression to over 10 GPa, with full recovery upon decompression. This work not only illustrated the relationship between piezofluorochromic performance with the detailed structural transformation under high pressure but also provided the strategy for the synthesis of mechanically ultrastable MOF materials.

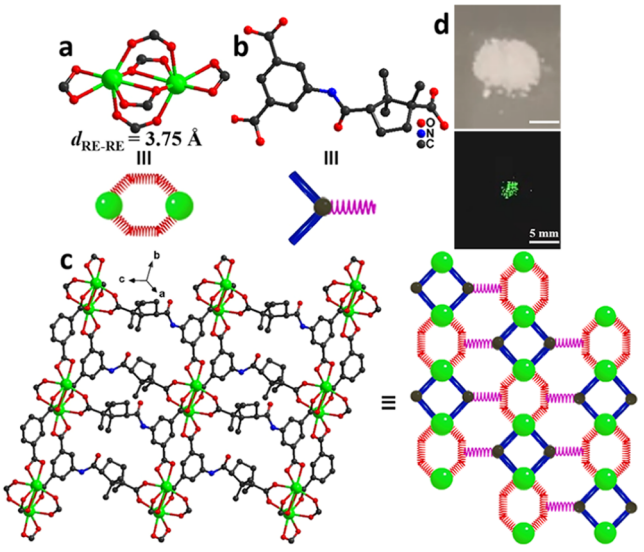

Figure 1. Schematic diagram and crystal structure of the binuclear RE center (a), the semiflexible ligand of *CAM*−*MBA*$^{3-}$ (b) and the 2D framework of RE-MOF (c). Hydrogen atoms were omitted for clarity. (d) Photo images of the mechano-luminescence from **Tb-MOF** upon manual squeezing.

RESULTS AND DISCUSSION

Single-crystal diffraction revealed that **Yb-MOF** crystallized in the chiral triclinic *P*1 space group,[33−35] where free DMF solvent molecules worked as the chiral factors to disrupt the crystal symmetry (Figures 1 and S1a, Tables S1 and S2). Each eight-coordinated Yb(III) with a distorted dodecahedral coordination geometry is bonded by five distinct carboxylate groups and one DMF solvent. The symmetric $Yb_2(COO)_4$ subunit with a Yb−Yb distance of 3.75 Å was connected by the bridging carboxylate groups with two Yb(III) ions, owing to μ_2-η^1:η^1 and μ_2-η^2:η^1-modes. **Yb-MOF** possessed a typical two-dimensional (2D) layer structure, where binuclear $Yb_2(COO)_4$ was interlocked by the ligand *CAM*−*MBA*$^{3-}$ (Figure 1). 2D layers were packed along the *a* direction to the resulting 3D structure (Figure S1). Unfortunately, no suitable crystal for **Tb-MOF** was obtained for single-crystal diffraction. However, powder X-ray diffraction (PXRD) analysis confirmed the isostructural nature of **Tb-MOF**, **Yb-MOF**, and bimetallic (**Tb_xYb_{2-x}**)**-MOF**, suggesting the same structural parameters for **Tb-MOF**, **Yb-MOF**, and bimetallic (**Tb_xYb_{2-x}**)**-MOF** (Figure S2). The composition of Tb(III) and Yb(III) in bimetallic (**Tb_xYb_{2-x}**)**-MOF** was examined by the ICP technique, as **$Tb_{0.86}Yb_{1.14}$-MOF** and **$Tb_{0.20}Yb_{1.80}$-MOF**, respectively (Table S3). Thermogravimetric analysis measurements indicated that the decomposition temperature of **Tb-MOF** was up to 460 °C (Figure S3).

The solid-state luminescent properties of **Tb-MOF** and (**Tb_xYb_{2-x}**)**-MOF** were first investigated at room temperature (Figure S4). Under the excitation at 365 nm, bright-green light emission was observed due to the characteristic emission transition of $^5D_4 \rightarrow {}^7F_J$ (J = 3−6) of the Tb(III) ions (Figure S4). Two intense emission bands at 487 and 544 nm corresponded to the electronic transitions from the excited state $^5D_4$ to the multiplets $^7F_6$ and $^7F_5$, while the relatively weak emission bands at 585 and 618 nm originated from $^5D_4 \rightarrow {}^7F_4$ and $^5D_4 \rightarrow {}^7F_3$ (Figure S4).[36−38] Moreover, the fluorescence intensity and lifetime significantly reduced after doping nonluminescent Yb(III) ions, where the lifetimes for **Tb-MOF**, **$Tb_{0.86}Yb_{1.14}$-MOF**, and **$Tb_{0.20}Yb_{1.80}$-MOF** were 976.4, 780.0, and 745.8 μs, respectively (Figure S4 and Table S4). These results were in agreement with previously reported Tb(III)-frameworks (Figure S4).[39−41]

The most striking feature of **Tb-MOF** was the mechano-luminescence (ML) property under low pressure, where a strong green emission was observed on manually squeezing the microcrystals between two glass slides (Figure 1). Further ML experiments were conducted for **Tb-MOF** embedded in the resin with different hardness (Figure S5). The ML of Tb-MOF embedded in the resin with high hardness was observed under 5 MPa compression (Figure S6). In contrast, a much weaker signal for Tb-MOF with a resin of less hardness was detected under 10 MPa compression (Figure S6). This suggested that the ML of **Tb-MOF** was induced by the fracture of **Tb-MOF** nanocrystals since the resin with less hardness could extend to resist the compression.

In contrast to **Tb-MOF**, the Yb-doped (**Tb_xYb_{2-x}**)**-MOF** showed no obvious ML under the same condition, which should be ascribed to the energy transfer between Tb(III) and nonluminescent Yb(III) ions.[29,42] To further understand the influence of the proportion of Yb on the ML, **$Tb_{1.78}Yb_{0.22}$-MOF** was further synthesized with less Yb(III) doping, and no ML was observed under the same condition. This might be

https://doi.org/10.1021/jacsau.4c00259
JACS Au 2024, 4, 2050−2057

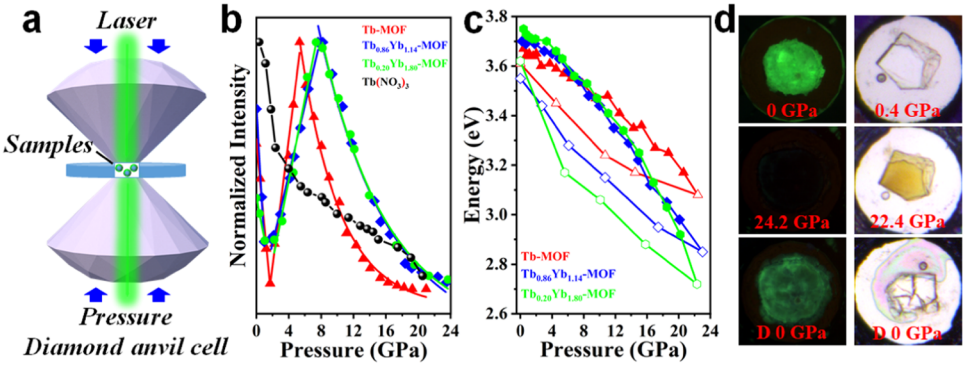

Figure 2. (a) Schematic diagram of a DAC used in high-pressure experiments. (b) Plots of *in situ*-normalized piezofluorochromic intensity with applied pressure. (c) Plots of band gap vs applied pressure, which were calculated from the *in situ* high-pressure UV absorption spectra. The filled and open symbols represent compression and decompression, respectively. (d) Visible images of **Tb-MOF** powder under excitation at 365 nm and the single crystal of **Tb-MOF** under indicated pressures. D represents decompression.

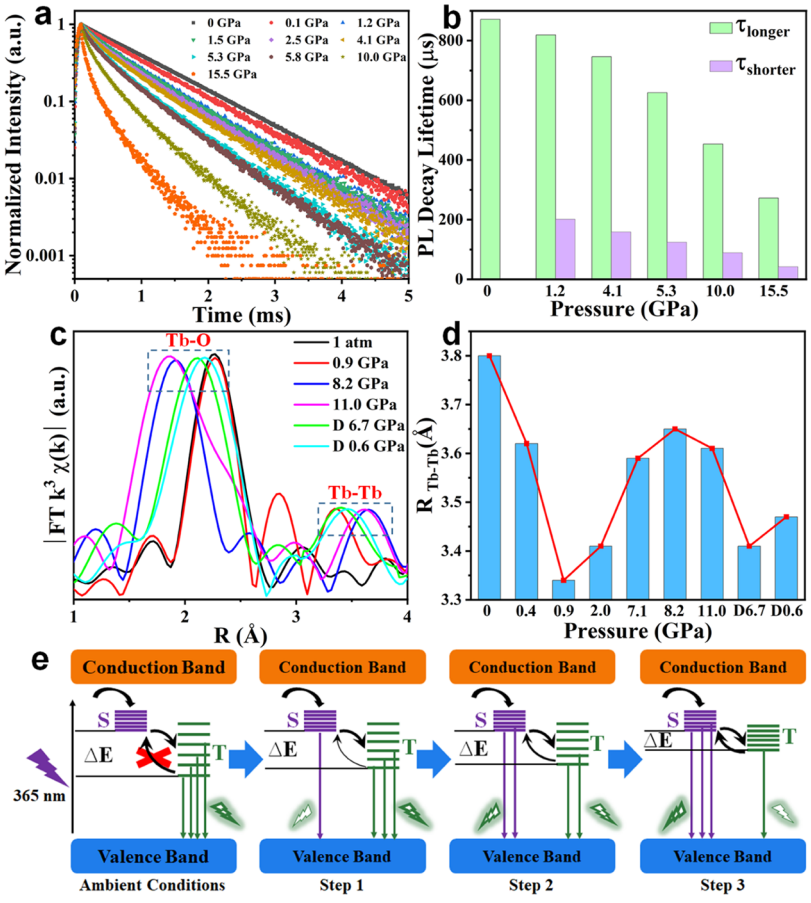

Figure 3. (a, b) Photoluminescence decay curves and the calculated decay constants from the longer and shorter lifetime for **Tb-MOF** under different pressures. (c, d) Fourier transform of k^2-weighted EXAFS for **Tb-MOF** and the indicated Tb−Tb distance under distinct pressures. D stands for decompression. (e) Energy-level change of **Tb-MOF** upon compression (S, spin-singlet states; T, spin-triplet states).

attributed to the $^5D_4$ excited energy level of Tb(III) being higher than the $^5F_{5/2}$ level of Yb(III); hence, excitons undergo a transition from the $^5D_4$ of Tb(III) to the $^5F_{5/2}$ of Yb(III) and then return to the ground state, resulting in the fluorescence quenching (Figure S8).[29] PXRD indicated that there was no significant structural change after the squeezing since the diffraction patterns for **Tb-MOF** were mainly retained (Figure S7). This interesting ML phenomenon of **Tb-MOF** was due to the crystallization in the piezoelectric *P*1 space group.[33−35]

Encouraged by the ML of **Tb-MOF**, a diamond anvil cell (DAC) was employed to generate quantifiable hydrostatic pressure, and the relationship between pressure and photoluminescent (PL) intensity of **Tb-MOF** was then investigated (Figure 2). The characteristic luminescence intensity at 544 nm of **Tb-MOF** was observed to first decrease with pressure, before increasing, and finally decreasing again (Figures 2 and S9). In the first region, 89% luminescence intensity linearly diminished under the relatively low pressure range (<1.7 GPa); in the second, the maximal intensity was reached at a pressure

https://doi.org/10.1021/jacsau.4c00259
JACS Au 2024, 4, 2050−2057

of 5.3 GPa, about 1.4-fold that of the pristine sample and 14.4-fold that of the minimum intensity at 1.7 GPa; in the third, a gradual decrease of the luminescence intensity fitting a negative exponential function was observed with further compression up to 23.2 GPa (Figure 2b). The luminescence was partially recovered after releasing the pressure, which suggested that the structural changes elicited by the compression to 23 GPa could not be fully eliminated (Figure S9). Moreover, no shift of the luminescent wavelength was observed during the whole compressing−decompressing process for **Tb-MOF**, which was ascribed to the characteristic luminescence from the Tb element (Figure S9).[43] The typical light-emitting materials were usually organic molecules, where the emission intensity changes under high-pressure compression were mainly due to the enhanced intermolecular interactions.

$Tb(NO_3)_3{\cdot}6H_2O$ was also investigated as the control sample to understand the subtle mechanism for the piezofluorochromism of **Tb-MOF** (Figures 2 and S10). A progressive fluorescence quenching process was detected for $Tb(NO_3)_3{\cdot}6H_2O$ with increasing applied pressure, *i.e.*, completely different behavior to that of **Tb-MOF**. In contrast to binuclear Tb(III) subunits in **Tb-MOF**, the single Tb(III) center was observed with a Tb−Tb distance of 6.7 Å, and no interaction between the neighboring Tb(III) could be induced even at 24.3 GPa (Figure S11). This may suggest that the Tb−Tb interaction would be responsible for the PL intensity change of **Tb-MOF** under compression.

In situ time-resolved PL decay kinetics of **Tb-MOF** under compression was further examined to explore the impact of pressure on the self-trapped exciton (STE) recombination rate of **Tb-MOF** (collected at 544 nm emission, Figure 3a). The PL decay constants are listed in Table S5. **Tb-MOF** indicated a single long PL lifetime of 871.4 μs in the DAC at ambient conditions, which was consistent with the typically observed slow $^5D_4 \rightarrow {}^7F_5$ transition emission in common Tb-based materials (976.4 μs).[44,45] Upon further compression, a short lifetime component with a decay time of less than 200 μs appeared in the decay curve and gradually occupied the dominant position, which resulted from the Tb−Tb interaction within the bimetallic $Tb_2(COO)_4$ unit upon compression (Table S5).[46] Both the long and short lifetime components progressively declined with increasing pressure, which suggested the onset of the interparticle interaction to contribute an additional STE emission behavior (Figure 3b).[47]

To understand the occurrence of a short lifetime, the detailed structure under compression of **Tb-MOF** was then examined. The crystallinity of **Tb-MOF** nanocrystals under compression was then first investigated by *in situ* high-pressure PXRD (Figure S12). The long-term order of the **Tb-MOF** framework was maintained up to 11.7 GPa since the diffraction pattern showed no obvious changes compared to the simulated one (Figure S12). Moreover, no new diffraction was observed up to 11.7 GPa, suggesting there was no phase transition of **Tb-MOF** and the long-term order was maintained. With further compression, **Tb-MOF** underwent amorphization at 13.8 GPa, and no obvious diffraction was observed. These suggested that the fluorescence changes under compression lower than 11 GPa were ascribed to local stretching of the binuclear $Tb_2(COO)_4$ unit.

Atomic pair distribution function (PDF) analysis could provide information about the short- and intermediate-range order in materials on the nanoscale, even for amorphous materials.[48] Long-distance oscillation peaks before the signal dampened to zero in the PDF show that the **Tb-MOF** retained the locally ordered structure even after amorphization over 13.8 GPa, which resulted in partial fluorescence recovery after the decompression (Figure S13 and Table S7). Meanwhile, the color of the **Tb-MOF** microsize single crystal also simultaneously turned from colorless at ambient pressure to light yellow under a pressure of 23.2 GPa, in which the crystal morphology did not change significantly, and reversed back to colorless after releasing the pressure (Figure 2d).

To elucidate the origin of the observed color change, *in situ* high-pressure absorption spectra of **Tb-MOF** were collected in DAC (Figure S14). At ambient conditions, **Tb-MOF** exhibited an obvious excitonic absorption peak at 315 nm (Figure S14). On increasing the pressure, the absorption peak experienced a persistent red shift up to a pressure of 22.4 GPa, which may be related to the dodecahedral shrinkage around Tb(III) ions (Figure S14). The coordination shrinkage would promote the overlap of Tb and O orbits, thus leading to the increase of electronic band dispersion, eventually resulting in a reduction of the band gap from 3.67 eV at ambient pressure to 3.08 eV at 22.4 GPa (Figures 2 and S14).[49−51] Moreover, after fully releasing the pressure, the absorption peak almost blue-shifted back to 316 nm, which suggested that the coordination environment of Tb(III) could be maintained during the whole compressing/decompressing process. In general, the sensitivity of the emission spectra to environmental changes is higher than that of the absorption spectra. For **Tb-MOF** under compression, the absorption indicated an obvious red shift, while the fluorescence remained unchanged. This is due to the fluorescence of **Tb-MOF** from the characteristic emission transition of $^5D_4 \rightarrow {}^7F_J$ (J = 3−6) of the Tb(III) ions with a fixed band-gap energy.[43]

This reversible shrinkage of the coordination environment around Tb(III) ions was further demonstrated by the *in situ* high-pressure FT-IR spectra (Figure S15), where the major absorption peaks in the range of 1800−1250 cm^{-1} were studied in detail. No obvious new peaks or shoulder peaks were observed with the pressure up to 9.7 GPa, and only a minor blue shift was found (Figure S15). In agreement with the UV absorption spectra, the FT-IR spectra were recovered after releasing the pressure. This reversible coordination shrinkage in **Tb-MOF** was ascribed to the flexibility of both the ligand *Cam*−*MBA*$^{3-}$ and binuclear $Tb_2(COO)_4$ clusters. Moreover, to further verify its reversibility, we recorded the fluorescence spectra of **Tb-MOF** during three consecutive compression−decompression cycles, which indicated that the framework has excellent flexibility (Figure S16).

According to previous reports, we speculated that both the transformations of the piezofluorochromic intensity and lifetime of **Tb-MOF** under compression resulted from the transition of Tb−Tb interactions. When 365 nm excitation was used under ambient conditions, the carriers in the ground states were excited to the STE singlet states and then underwent a fast intersystem crossing (ISC) from the singlet states to the triplet states; moreover, the strong and long-lifetime phosphorescence was generated from the radiation decay of the triplet exciton, which is the characteristic luminescence of rare-earth ions (Figure 3e).[52,53] At lower pressures (<1.7 GPa), the Tb−Tb interaction was enhanced due to the shortened distance, where the overlapping of the electron clouds of Tb(III) could occur and lead to a decrease of the highest occupied molecular orbital (HOMO)−least

https://doi.org/10.1021/jacsau.4c00259
JACS Au 2024, 4, 2050−2057

unoccupied molecular orbital (LUMO) gap of the binuclear Tb cluster and the appearance of a short lifetime component in the decay curve.[42,46] Thus, the nonradiative excitation electron transfer effectively deactivated the radiation energy and weakened the emission (Figure 3e Step 1), which was consistent with the observation for the $Au_{60}S_7(SCH_2Ph)_{36}$ nanocluster.[46] The electrostatic repulsion from Tb(III) ions then turned into the dominant force to overcome the influence from the compression up to 5.3 GPa, and the Tb−Tb interaction was weakened due to the elongated distance, where the intensity of the emission was enhanced. However, external pressure reduced the difference energy ΔE (the balance between the singlet and triplet states), which promoted the pressure-driven reverse intersystem crossing (RISC) from long-lived triplet excited states back to short-lived singlet excited states, leading to the lifetime being shortened (Figure 3e Step 2).[47,54,55] Thus, the shortened lifetime fluorescence upon compression was attributed to the thermal activated delayed fluorescence (TADF), which refers to the low-energy triplet excitons transiting to the singlet state through RISC, followed by radiative transitions back to the ground state.[47,56] Once the pressure went beyond 5.3 GPa, the compression reversed back to be the dominant force, Tb−Tb interactions were enhanced again, and ΔE further decreased, resulting in a progressively weakened intensity and lifetime (Figure 3e Step 3).

In order to demonstrate our hypothesis and quantify the dynamic shrinkage of binuclear $Tb_2(COO)_4$ clusters under pressure, *in situ* high-pressure X-ray absorption spectroscopy (XAS) measurements with smaller compression steps were carried out up to 10 GPa since the dual inflection point behavior for **Tb-MOF** fluorescence intensity occurred at less than 10 GPa (Figures 3, S17, and S18). *In situ* X-ray absorption near-edge structure (XANES) of the Tb L_3-edge indicated that the pressure-dependent XANES curves of Tb-MOF overlapped with the curves of the pristine sample and the control sample Tb_2O_3, suggesting that the oxidation state of the Tb element retained the same trivalent state during the compressing and decompressing process (Figure S17).[57−59]

The coordination environment and neighboring interatomic distances of Tb(III) in **Tb-MOF** were further analyzed by extended X-ray absorption fine structure (EXAFS) (Figure S18). In the ambient state, two obvious peaks at 2.27 and 3.80 Å were observed for **Tb-MOF**, which were attributed to Tb−O and Tb−Tb scattering paths and were similar to 2.24 and 3.63 Å observed in Tb_2O_3 (Figure S18). Due to the complexity of Tb−O bonds, Tb−Tb bond lengths were calculated to reflect the influence of compression, which was also highly related to the piezofluorochromic performance of **Tb-MOF**. Tb−Tb distance upon compression indicated the same tendency as the piezofluorochromic intensity under compression, as dropping from 3.80 to 3.34 Å at 0.9 GPa, then increasing to 3.65 Å at 8.2 GPa, and further decreasing to 3.61 Å at 11.0 GPa (Figure 3d and Table S6). More importantly, after releasing the pressure to 0.6 GPa, the Tb−Tb distance reversed back to 3.47 Å, which was very close to the length in the first compression at 1.1 GPa. The observation confirmed that the piezofluorochromic performance of **Tb-MOF** was ascribed to the transition of the Tb−Tb interaction upon compression, and **Tb-MOF** could retain the intact framework up to 10 GPa. Compared to the other reported MOFs, **Tb-MOF** possessed ultrastable mechanical stability (Figure 4 and Table S8).[2,16,17,20,43,60−70]

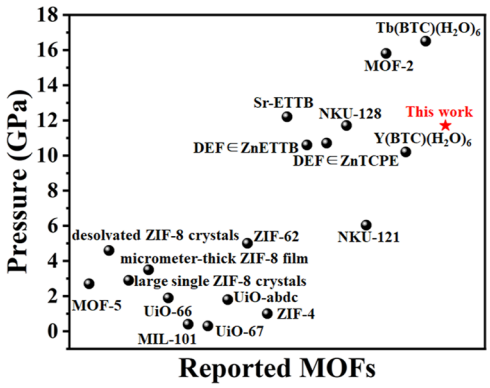

Figure 4. Mechanical stability of **Tb-MOF** compared to those of other reported MOFs.

In addition, the energy transfer from ligand to metal is also critical for Tb-MOF fluorescence since the fluorescence energy of **Tb-MOF** was from the transfer from the excited ligand.[71−73] To assess the efficiency of the energy transfer from ligand to metal, *in situ* high-pressure absorption spectra for the ligand *H_3CAM−MBA* were then conducted (Figure S19). With the pressure increasing, the absorption peak gradually red-shifted, and the optical band gap decreased linearly, suggesting that the excited level of the ligand *H_3CAM−MBA* was downregulated with compression. This was inconsistent with the observed double inflection point behavior of **Tb−MOF** under compression, which suggested that the energy transfer from the ligand to the Tb(III) ion was not directly correlated with the fluorescence evolution of **Tb-MOF** upon compression. Thus, the influence of the fluorescence intensity of **Tb-MOF** was mainly due to the stretching of the Tb−Tb distance upon compression.

To further demonstrate the conclusion that the difference energy ΔE (the balance between the singlet and triplet states) decreases under high pressure, the theoretical calculation of the HOMO−LUMO band-gap value of the binuclear $Tb_2(COO)_4$ molecule with different Tb−Tb distances was investigated with the ORCA software.[74−76] To mimic the binuclear $Tb_2(COO)_4$ unit, formic acid was used to construct the $Tb_2(HCOO)_4$ single molecule. With the shortened Tb−Tb distance, the greater number of electron clouds overlapping the Tb(III) ions resulted in a decrease of the HOMO−LUMO gap of the binuclear cluster (Figure S20). As the Tb−Tb distance shortened from the initial 3.80 Å to the shortest 3.40 Å, the HOMO−LUMO band gap decreased from 5.84 to 4.80 eV (Table S10). Thus, the dual inflection point behavior for the **Tb-MOF** fluorescence intensity under compression was highly related to the stretchable Tb−Tb distance in **Tb-MOF**.

Furthermore, a similar phenomenon was observed for Yb-doped **(Tb_xYb_{2-x})-MOF**, suggesting the existence of Tb(III) was mainly responsible for the piezofluorochromism (Figures 2, S21−S25, Table S9). The minor differences should result from the distinct content of Tb(III) in Yb-doped bimetallic **(Tb_xYb_{2-x})-MOF**.

CONCLUSIONS

In summary, we have reported a smart 2D piezoelectrochromic chiral Tb framework, which could stabilize under ultrahigh pressure up to 10 GPa. **Tb-MOF** microcrystals indicated intriguing mechano-luminescence under manual squeezing due to crystallization in the piezoelectric *P*1 space group. Upon

https://doi.org/10.1021/jacsau.4c00259
JACS Au 2024, 4, 2050−2057

high-pressure compression in the DAC, **Tb-MOF** exhibited characteristic Tb(III) luminescence with the intensity tendency of decreasing−increasing−decreasing and a progressively shortening lifetime. *In situ* high-pressure XAS demonstrated that the photoluminescence transformation during the compression was ascribed to the stretchability of Tb−Tb interaction. *In situ* high-pressure UV absorption spectra and FT-IR demonstrated the reversible coordination environment transformation around the center Tb(III) in **Tb-MOF** upon compression/decompression. We used a chiral semiflexible ligand to construct an ideal platform for exploring the influence of metal nodes on the fluorescence performance of MOF materials under external pressure. This work not only provided the mechanism of high-pressure luminescence for RE-MOF but also illustrated the relationship of the piezofluorochromic performance with the detailed structural transformation for the first time.

■ ASSOCIATED CONTENT

Supporting Information

The Supporting Information is available free of charge at https://pubs.acs.org/doi/10.1021/jacsau.4c00259.

Experimental procedures; PXRD; 3D structure of **Yb-MOF;** *in situ* high-pressure PL spectra; UV absorption spectra; and FT-IR spectra (PDF)
Yb-MOF (CIF)

■ AUTHOR INFORMATION

Corresponding Authors

Jiangwei Zhang − *College of Chemistry and Chemical Engineering, Inner Mongolia University, Hohhot 010021, China;* orcid.org/0000-0002-1221-3033; Email: jwzhang@dicp.ac.cn

Zhiqiang Chen − *Center for High Pressure Science and Technology Advanced Research, Shanghai 201203, China;* Email: chenzq@hpstar.ac.cn

Zhi Su − *Jiangsu Collaborative Innovation Center of Biomedical Functional Materials, Jiangsu Key Laboratory of Biofunctional Materials, College of Chemistry and Materials Science, Nanjing Normal University, Nanjing 210046, China;* orcid.org/0000-0002-1339-0525; Email: zhisu@njnu.edu.cn

Authors

Ziyou Zhang − *Jiangsu Collaborative Innovation Center of Biomedical Functional Materials, Jiangsu Key Laboratory of Biofunctional Materials, College of Chemistry and Materials Science, Nanjing Normal University, Nanjing 210046, China; Center for High Pressure Science and Technology Advanced Research, Shanghai 201203, China;* orcid.org/0009-0005-0323-4202

Dongping Deng − *Jiangsu Collaborative Innovation Center of Biomedical Functional Materials, Jiangsu Key Laboratory of Biofunctional Materials, College of Chemistry and Materials Science, Nanjing Normal University, Nanjing 210046, China*

Xiaoqian Xu − *Jiangsu Collaborative Innovation Center of Biomedical Functional Materials, Jiangsu Key Laboratory of Biofunctional Materials, College of Chemistry and Materials Science, Nanjing Normal University, Nanjing 210046, China*

Shuai Yan − *Shanghai Synchrotron Radiation Facility, Institute of Applied Physics, Chinese Academy of Sciences, Shanghai 201204, China*

Zhiying Guo − *Beijing Synchrotron Radiation Facility, Institute of High Energy Physics, Chinese Academy of Sciences, Beijing 100049, China;* orcid.org/0000-0001-5904-3409

Hongliang Dong − *Center for High Pressure Science and Technology Advanced Research, Shanghai 201203, China*

Complete contact information is available at: https://pubs.acs.org/10.1021/jacsau.4c00259

Author Contributions

#Z.Z., D.D., and X.X. authors contributed equally.

Funding

The authors appreciate the financial support from the National Natural Science Foundation of China (NSFC) (Grant Nos. 22277056, U1530402), the Distinguished Young Scholars of Jiangsu Province (BK20230006), and the Postgraduate Research & Practice Innovation of Jiangsu Province for ZZY (KYCX22_1548).

Notes

The authors declare no competing financial interest.

■ ACKNOWLEDGMENTS

The authors thank Xujie Lv and Yonggang Wang from the Center for High Pressure Science and Technology Advanced Research (HPSTAR) for the support on the *in situ* high-pressure fluorescence measurements and the staff scientists of BL05U, BL06B, and BL15U beamlines at the Shanghai Synchrotron Radiation Facility (SSRF) for the assistance during data collection.

■ REFERENCES

(1) Chen, C. X.; Wei, Z. W.; Fan, Y. N.; Su, P. Y.; Ai, Y. Y.; Qiu, Q. F.; Wu, K.; Yin, S. Y.; Pan, M.; Su, C. Y. Visualization of anisotropic and stepwise piezofluorochromism in an MOF single crystal. *Chem* **2018**, *4*, 2658−2669.

(2) Guo, X. L.; Zhu, N. S.; Wang, S. P.; Li, G. H.; Bai, F. Q.; Li, Y.; Han, Y. H.; Zou, B.; Chen, X. B.; Shi, Z.; Feng, S. H. Stimuli-responsive luminescent properties of tetraphenylethene-based strontium and cobalt metal-organic frameworks. *Angew. Chem., Int. Ed.* **2020**, *59*, 19716−19721.

(3) Li, H. Y.; Zhao, S. N.; Zang, S. Q.; Li, J. Functional metal-organic frameworks as effective sensors of gases and volatile compounds. *Chem. Soc. Rev.* **2020**, *49*, 6364−6401.

(4) Lin, R. B.; Liu, S. Y.; Ye, J. W.; Li, X. F.; Zhang, J. P. Photoluminescent metal-organic frameworks for gas sensing. *Adv. Sci.* **2016**, *3*, No. 1500434.

(5) Zhang, Q.; Su, J.; Feng, D. W.; Wei, Z. W.; Zou, X. D.; Zhou, H. C. Piezofluorochromic metal-organic framework: a microscissor lift. *J. Am. Chem. Soc.* **2015**, *137*, 10064−10067.

(6) Allendorf, M. D.; Houk, R. J. T.; Andruszkiewicz, L.; Talin, A. A.; Pikarsky, J.; Choudhury, A.; Gall, K. A.; Hesketh, P. J. Stress-induced chemical detection using flexible metal-organic frameworks. *J. Am. Chem. Soc.* **2008**, *130*, 14404−14405.

(7) Irie, M.; Fukaminato, T.; Sasaki, T.; Tamai, N.; Kawai, T. A digital fluorescent molecular photoswitch. *Nature* **2002**, *420*, 759−760.

(8) Chen, C. X.; Yin, S. Y.; Wei, Z. W.; Qiu, Q. F.; Zhu, N. X.; Fan, Y. N.; Pan, M.; Su, C. Y. Pressure-induced multiphoton excited fluorochromic metal-organic frameworks for improving MPEF properties. *Angew. Chem., Int. Ed.* **2019**, *58*, 14379−14385.

(9) Chi, Z. G.; Zhang, X. Q.; Xu, B. J.; Zhou, X.; Ma, C. P.; Zhang, Y.; Liu, S. W.; Xu, J. R. Recent advances in organic mechanofluorochromic materials. *Chem. Soc. Rev.* **2012**, *41*, 3878−3896.

(10) Dong, Y. J.; Zhang, J. B.; Tan, X.; Wang, L. J.; Chen, J. L.; Li, B.; Ye, L.; Xu, B.; Zou, B.; Tian, W. Multi-stimuli responsive fluorescence switching: the reversible piezochromism and protonation effect of a divinylanthracene derivative. *J. Mater. Chem. C* **2013**, *1*, 7554−7559.
(11) Younis, S. A.; Bhardwaj, N.; Bhardwaj, S. K.; Kim, K.-H.; Deep, A. Rare earth metal-organic frameworks (RE-MOFs): synthesis, properties, and biomedical applications. *Coord. Chem. Rev.* **2021**, *429*, No. 213620.
(12) Saraci, F.; Quezada-Novoa, V.; Donnarumma, P. R.; Howarth, A. J. Rare-earth metal-organic frameworks: from structure to applications. *Chem. Soc. Rev.* **2020**, *49*, 7949−7977.
(13) Robison, L.; Drout, R. J.; Redfern, L. R.; Son, F. A.; Wasson, M. C.; Goswami, S.; Chen, Z. J.; Olszewski, A.; Idrees, K. B.; Islamoglu, T.; Farha, O. K. Designing porous materials to resist compression: mechanical reinforcement of a Zr-MOF with structural linkers. *Chem. Mater.* **2020**, *32*, 3545−3552.
(14) Redfern, L. R.; Ducamp, M.; Wasson, M. C.; Robison, L.; Son, F. A.; Coudert, F.-X.; Farha, O. K. Isolating the role of the node-linker bond in the compression of UiO-66 metal-organic frameworks. *Chem. Mater.* **2020**, *32*, 5864−5871.
(15) Redfern, L. R.; Farha, O. K. Mechanical properties of metal-organic frameworks. *Chem. Sci.* **2019**, *10*, 10666−10679.
(16) Zhu, Z. H.; Bi, C. J.; Zou, H. H.; Feng, G. X.; Xu, S. P.; Tang, B. Z. Smart tetraphenylethene-based luminescent metal-organic frameworks with amide-assisted thermofluorochromics and piezofluorochromics. *Adv. Sci.* **2022**, *9*, No. 2200850.
(17) Su, Z.; Miao, Y. R.; Zhang, G. H.; Miller, J. T.; Suslick, K. S. Bond breakage under pressure in a metal organic framework. *Chem. Sci.* **2017**, *8*, 8004−8011.
(18) Chen, Z. H.; Gallo, G.; Sawant, V. A.; Zhang, T. X.; Zhu, M. L.; Liang, L. L.; Chanthapally, A.; Bolla, G.; Quah, H. S.; Liu, X. G.; Loh, K. P.; Dinnebier, R. E.; Xu, Q. H.; Vittal, J. J. Giant enhancement of second harmonic generation accompanied by the structural transformation of 7-fold to 8-fold interpenetrated metal-organic frameworks (MOFs). *Angew. Chem., Int. Ed.* **2020**, *59*, 833−838.
(19) Gupta, M.; Vittal, J. J. Control of interpenetration and structural transformations in the interpenetrated MOFs. *Coord. Chem. Rev.* **2021**, *435*, No. 213789.
(20) Hobday, C. L.; Marshall, R. J.; Murphie, C. F.; Sotelo, J.; Richards, T.; Allan, D. R.; Düren, T.; Coudert, F. X.; Forgan, R. S.; Morrison, C. A.; Moggach, S. A.; Bennett, T. D. A computational and experimental approach linking disorder, high-pressure behavior, and mechanical properties in UiO frameworks. *Angew. Chem., Int. Ed.* **2016**, *55*, 2401−2405.
(21) Karadeniz, B.; Žilić, D.; Huskić, I.; Germann, L. S.; Fidelli, A. M.; Muratović, S.; Lončarić, I.; Etter, M.; Dinnebier, R. E.; Barišić, D.; Cindro, N.; Islamoglu, T.; Farha, O. K.; Friščić, T.; Užarević, K. Controlling the polymorphism and topology transformation in porphyrinic zirconium metal-organic frameworks via mechanochemistry. *J. Am. Chem. Soc.* **2019**, *141*, 19214−19220.
(22) Redfern, L. R.; Robison, L.; Wasson, M. C.; Goswami, S.; Lyu, J.; Islamoglu, T.; Chapman, K. W.; Farha, O. K. Porosity dependence of compression and lattice rigidity in metal-organic framework series. *J. Am. Chem. Soc.* **2019**, *141*, 4365−4371.
(23) Nishida, J. I.; Ohura, H.; Kita, Y.; Hasegawa, H.; Kawase, T.; Takada, N.; Sato, H.; Sei, Y.; Yamashita, Y. Phthalimide compounds containing a trifluoromethylphenyl group and electron-donating aryl groups: color-tuning and enhancement of triboluminescence. *J. Org. Chem.* **2016**, *81*, 433−441.
(24) Fontenot, R. S.; Bhat, K. N.; Owens, C. A.; Hollerman, W. A.; Aggarwal, M. D. Effects of added dibutyl phosphate on the luminescent properties of europium tetrakis dibenzoylmethide triethylammonium. *J. Lumin.* **2015**, *158*, 428−434.
(25) Xu, S. D.; Liu, T. T.; Mu, Y. X.; Wang, Y. F.; Chi, Z. G.; Lo, C. C.; Liu, S. W.; Zhang, Y.; Lien, A.; Xu, J. R. An organic molecule with asymmetric structure exhibiting aggregation-induced emission, delayed fluorescence, and mechanoluminescence. *Angew. Chem.* **2015**, *127*, 888−892.
(26) Fang, M. M.; Yang, J.; Liao, Q. Y.; Gong, Y. B.; Xie, Z. L.; Chi, Z. G.; Peng, Q.; Lia, Q. Q.; Li, Z. Triphenylamine derivatives: different molecular packing and the corresponding mechanoluminescent or mechanochromism property. *J. Mater. Chem. C* **2017**, *5*, 9879−9885.
(27) Rheingold, A. L.; King, W. Crystal structures of three brilliantly triboluminescent centrosymmetric lanthanide complexes: piperidinium tetrakis(benzoylacetonato)europate, Hexakis(antipyrine) terbium triiodide, and hexaaquadichloroterbium chloride. *Inorg. Chem.* **1989**, *28*, 1715−1719.
(28) Chen, X. F.; Zhu, X. H.; Xu, Y. H.; Raj, S. S. S.; Öztürk, S.; Fun, H. K.; Mac, J.; You, X. Z. Triboluminescence and crystal structures of non-ionic europium complexes. *J. Mater. Chem.* **1999**, *9*, 2919−2922.
(29) Xie, Y. J.; Li, Z. Triboluminescence: Recalling interest and new aspects. *Chem* **2018**, *4*, 943−971.
(30) Nakayama, H.; Nishida, J.; Takada, N.; Sato, H.; Yamashita, Y. Crystal structures and triboluminescence based on trifluoromethyl and pentafluorosulfanyl substituted asymmetric N-phenyl imide compounds. *Chem. Mater.* **2012**, *24*, 671−676.
(31) Zeng, Y. L.; Huang, X. Q.; Huang, C. R.; Zhang, H.; Wang, F.; Wang, Z. X. Unprecedented 2D homochiral hybrid lead-iodide perovskite thermochromic ferroelectrics with ferroelastic switching. *Angew. Chem., Int. Ed.* **2021**, *60*, 10730−10735.
(32) Zhang, Z. X.; Song, X. J.; Li, Y. R.; Chen, X. G.; Zhang, Y.; Lv, H. P.; Tang, Y. Y.; Xiong, R. G.; Zhang, H. Y. The first chiro-inositol organosilicon ferroelectric crystal. *Angew. Chem.* **2022**, *134* (44), e202210809 DOI: 10.1002/ange.202210809.
(33) Yuan, C.; Li, X.; Semin, S.; Feng, Y.; Rasing, T.; Xu, J. Chiral lead halide perovskite nanowires for second-order nonlinear optics. *Nano Lett.* **2018**, *18*, 5411−5417.
(34) Wojtaś, M.; Gągorb, A.; Kholkin, A. L. Strong piezoelectricity in [H-β-(2-pyridyl)-Ala-OH][BF_4] and [H-β-(2-pyridyl)-Ala-OH]-[ClO_4]-new amino acid based hybrid crystals. *J. Mater. Chem. C* **2016**, *4*, 7622−7631.
(35) Zhang, W.; Xiong, R. G. Ferroelectric metal-organic frameworks. *Chem. Rev.* **2012**, *112*, 1163−1195.
(36) Zhao, D.; Yue, D.; Jiang, K.; Zhang, L.; Li, C. X.; Qian, G. D. Isostructural Tb^{3+}/Eu^{3+} co-doped metal-organic framework based on pyridine-containing dicarboxylate ligands for ratiometric luminescence temperature sensing. *Inorg. Chem.* **2019**, *58*, 2637−2644.
(37) Wang, Y. T.; Zhang, K.; Wang, X. K.; Xin, X. L.; Zhang, X. R.; Fan, W. D.; Xu, B.; Dai, F. N.; Sun, D. F. Accurate tuning of rare earth metal-organic frameworks with unprecedented topology for white-light emission. *J. Mater. Chem. C* **2020**, *8*, 1374−1379.
(38) Lei, M. Y.; Ge, F. Y.; Gao, X. J.; Shi, Z. Q.; Zheng, H. G. A water-stable Tb-MOF as a rapid, accurate, and highly sensitive ratiometric luminescent sensor for the discriminative sensing of antibiotics and D_2O in H_2O. *Inorg. Chem.* **2021**, *60*, 10513−10521.
(39) Qu, X. L.; Yan, B. Stable Tb(III)-based metal-organic framework: structure, photoluminescence, and chemical sensing of 2-thiazolidinethione-4-carboxylic acid as a biomarker of CS_2. *Inorg. Chem.* **2019**, *58*, 524−534.
(40) Min, H.; Han, Z. S.; Wang, M. M.; Li, Y. J.; Zhou, T. Z.; Shi, W.; Cheng, P. A water-stable terbium metal-organic framework as a highly sensitive fluorescent sensor for nitrite. *Inorg. Chem. Front.* **2020**, *7*, 3379−3385.
(41) Jia, P.; Gao, L.; Zheng, Y.; Zheng, X.; Wang, C.; Yang, C. L.; Li, Y. B.; Zhao, Y. L. Ultrastable Tb-organic framework as a selective sensor of phenylglyoxylic acid in urine. *ACS Appl. Mater. Interfaces* **2021**, *13*, 33546−33556.
(42) Hirai, Y.; Nakanishi, T.; Kitagawa, Y.; Fushimi, K.; Seki, T.; Ito, H.; Hasegawa, Y. Triboluminescence of lanthanide coordination polymers with face-to-face arranged substituents. *Angew. Chem., Int. Ed.* **2017**, *56*, 7171−7175.
(43) Wang, Y. X.; Yang, X. Y.; Liu, C.; Liu, Z. D.; Fang, Q. R.; Bai, F. Q.; Wang, S. P.; Hou, X. Y.; Feng, B. T.; Chen, B. L.; Zou, B. Maximized green photoluminescence in Tb-based metal-organic framework via pressure-treated engineering. *Angew. Chem.* **2022**, *134* (48), e202210836 DOI: 10.1002/ange.202210836.

(44) Li, A.; Li, F.; Chen, Y.; Xie, Y.; Li, X.; Liu, X.; Xu, S.; Xu, W.; Wang, J.; Li, Z. Flexible and continuous regulation promoting remarkably emission enhancement of planar triphenylene. *ACS Mater. Lett.* **2022**, *4*, 2151−2158.
(45) Yu, X.; Ryadun, A. A.; Potapov, A. S.; Fedin, V. P. Ultra-low limit of luminescent detection of gossypol by terbium(III)-based metal-organic framework. *J. Hazard. Mater.* **2023**, *452*, No. 131289.
(46) Gan, Z. B.; Liu, Y. G.; Wang, L.; Jiang, S. Q.; Xia, N.; Yan, Z. P.; Wu, X.; Zhang, J. R.; Gu, W. M.; He, L. Z.; Dong, J. W.; Ma, X. D.; Kim, J.; Wu, Z. Y.; Xu, Y. X.; Li, Y. C.; Wu, Z. K. Distance makes a difference in crystalline photoluminescence. *Nat. Commun.* **2020**, *11*, No. 5572.
(47) Ma, Z. W.; Li, Q.; Luo, J. J.; Li, S. R.; Sui, L. Z.; Zhao, D. L.; Yuan, K. J.; Xiao, G. J.; Tang, J.; Quan, Z. W.; Zou, B. Pressure-driven reverse intersystem crossing: new path toward bright deep-blue emission of lead-free halide double perovskites. *J. Am. Chem. Soc.* **2021**, *143*, 15176−15184.
(48) Terban, M. W.; Billinge, S. J. L. Structural analysis of molecular materials using the pair distribution function. *Chem. Rev.* **2022**, *122*, 1208−1272.
(49) Fu, R. J.; Zhao, W. Y.; Wang, L. R.; Ma, Z. W.; Xiao, G. J.; Zou, B. Pressure-induced emission toward harvesting cold white light from warm white light. *Angew. Chem., Int. Ed.* **2021**, *60*, 10082−10088.
(50) Sun, M. E.; Geng, T.; Yong, X.; Lu, S. Y.; Ai, L.; Xiao, G. J.; Cai, J. M.; Zou, B.; Zang, S. Q. Pressure-triggered blue emission of zero-dimensional organic bismuth bromide perovskite. *Adv. Sci.* **2021**, *8*, No. 2004853.
(51) Zhang, L.; Fang, Y. Y.; Sui, L. Z.; Yan, J. J.; Wang, K.; Yuan, K. J.; Mao, W. L.; Zou, B. Tuning emission and electron-phonon coupling in lead-free halide double perovskite $Cs_2AgBiCl_6$ under pressure. *ACS Energy Lett.* **2019**, *4*, 2975−2982.
(52) Liang, L.; Chen, J.; Shao, K.; Qin, X.; Pan, Z.; Liu, X. Controlling persistent luminescence in nanocrystalline phosphors. *Nat. Mater.* **2023**, *22*, 289−304.
(53) Liu, X.; Liao, Q.; Yang, J.; Li, Z.; Li, Q. Unveiling one-to-one correspondence between excited triplet states and determinate interactions by temperature-controllable blue-green-yellow afterglow. *Angew. Chem., Int. Ed.* **2023**, *62* (24), No. e202302792, DOI: 10.1002/anie.202302792.
(54) Liu, S. P.; Yang, B.; Chen, J. S.; Wei, D. H.; Zheng, D. Y.; Kong, Q. K.; Deng, W. Q.; Han, K. L. Efficient thermally activated delayed fluorescence from all-inorganic cesium zirconium halide perovskite nanocrystals. *Angew. Chem., Int. Ed.* **2020**, *59*, 21925−21929.
(55) Knowles, K. E.; Nelson, H. D.; Kilburn, T. B.; Gamelin, D. R. Singlet-triplet splittings in the luminescent excited states of colloidal Cu^+: CdSe, Cu^+: InP, and $CuInS_2$ nanocrystals: charge transfer configurations and self-trapped excitons. *J. Am. Chem. Soc.* **2015**, *137*, 13138−13147.
(56) Liu, Y.; Li, C.; Ren, Z.; Yan, S.; Bryce, M. R. All-organic thermally activated delayed fluorescence materials for organic light-emitting diodes. *Nat. Rev. Mater.* **2018**, *3*, 18020.
(57) Boglaienko, D.; Andersenb, A.; Healdc, S. M.; Vargab, T.; Mortensend, D. R.; Tetefe, S.; Seidlere, G. T.; Govindf, N.; Levitskaia, T. G. X-ray absorption spectroscopy of trivalent Eu, Gd, Tb, and Dy chlorides and oxychlorides. *J. Alloys Compd.* **2022**, *897*, No. 162629.
(58) Rice, N. T.; Popov, I. A.; Russo, D. R.; Bacsa, J.; Batista, E. R.; Yang, P.; Telser, J.; Pierre, H. S. L. Design, isolation, and spectroscopic analysis of a tetravalent terbium complex. *J. Am. Chem. Soc.* **2019**, *141*, 13222−13233.
(59) Fieser, M. E.; Ferrier, M. G.; Su, J.; Batista, E.; Cary, S. K.; Engle, J. W.; Evans, W. J.; Pacheco, J. S. L.; Kozimor, S. A.; Olson, A. C.; Ryan, A. J.; Stein, B. W.; Wagner, G. L.; Woen, D. H.; Vitovae, T.; Yang, P. Evaluating the electronic structure of formal Ln^{II} ions in $Ln^{II}(C_5H_4SiMe_3)_3^{1-}$ using XANES spectroscopy and DFT calculations. *Chem. Sci.* **2017**, *8*, 6076−6091.
(60) Bahr, D. F.; Reid, J. A.; Mook, W. M.; Bauer, C. A.; Stumpf, R.; Skulan, A. J.; Moody, N. R.; Simmons, B. A.; Shindel, M. M.; Allendorf, M. D. Mechanical properties of cubic zinc carboxylate IRMOF-1 metal-organic framework crystals. *Phys. Rev. B* **2007**, *76*, No. 184106.
(61) Su, Z.; Miao, Y. R.; Mao, S. M.; Zhang, G. H.; Dillon, S.; Miller, J. T.; Suslick, K. S. Compression-induced deformation of individual metal-organic framework microcrystals. *J. Am. Chem. Soc.* **2015**, *137*, 1750−1753.
(62) Tan, J. C.; Bennett, T. D.; Cheetham, A. K. Chemical structure, network topology, and porosity effects on the mechanical properties of zeolitic imidazolate frameworks. *Proc. Natl. Acad. Sci. U.S.A.* **2010**, *107*, 9938−9943.
(63) Eslava, S.; Zhang, L.; Esconjauregui, S.; Yang, J.; Vanstreels, K.; Baklanov, M. R.; Saiz, E. Metal-organic framework ZIF-8 films as low-κ dielectrics in microelectronics. *Chem. Mater.* **2013**, *25*, 27−33.
(64) Celeste, A.; Paolone, A.; Itie, J. P.; Borondics, F.; Joseph, B.; Grad, O.; Blanita, G.; Zlotea, C.; Capitani, F. Mesoporous metal-organic framework MIL-101 at high pressure. *J. Am. Chem. Soc.* **2020**, *142*, 15012−15019.
(65) Widmer, R. N.; Lampronti, G. I.; Anzellini, S.; Gaillac, R.; Farsang, S.; Zhou, C.; Belenguer, A. M.; Wilson, C. W.; Palmer, H.; Kleppe, A. K.; Wharmby, M. T.; Yu, X.; Cohen, S. M.; Telfer, S. G.; Redfern, S. A. T.; Coudert, F.-X.; MacLeod, S. G.; Bennett, T. D. Pressure promoted low-temperature melting of metal-organic frameworks. *Nat. Mater.* **2019**, *18*, 370−376.
(66) Bennett, T. D.; Simoncic, P.; Moggach, S. A.; Gozzo, F.; Macchi, P.; Keen, D. A.; Tan, J.-C.; Cheetham, A. K. Reversible pressure-induced amorphization of a zeolitic imidazolate framework (ZIF-4). *Chem. Commun.* **2011**, *47*, 7983−7985.
(67) Yao, Z. Q.; Wang, K.; Liu, R.; Yuan, Y. J.; Pang, J. J.; Li, Q. W.; Shao, T. Y.; Li, Z. G.; Feng, R.; Zou, B.; Li, W.; Xu, J.; Bu, X. H. Dynamic full-color tuning of organic chromophore in a multi-stimuli-responsive 2D flexible MOF. *Angew. Chem., Int. Ed.* **2022**, *61* (17), e202202073 DOI: 10.1002/anie.202202073.
(68) Yao, Z. Q.; Xu, J.; Zou, B.; Hu, Z. P.; Wang, K.; Yuan, Y. J.; Chen, Y. P.; Feng, R.; Xiong, J. B.; Hao, J. L.; Bu, X. H. A dual-stimuli-responsive coordination network featuring reversible wide-range luminescence-tuning behavior. *Angew. Chem., Int. Ed.* **2019**, *58*, 5614−5618.
(69) Zhang, T.; Yong, X.; Yu, J. K.; Wang, Y. X.; Wu, M.; Yang, Q.; Hou, X. Y.; Liu, Z. D.; Wang, K.; Yang, X. Y.; Lu, S. Y.; Zou, B. Brightening blue photoluminescence in nonemission MOF-2 by pressure treatment engineering. *Adv. Mater.* **2023**, *35*, No. 2211729.
(70) Wang, Y. X.; Liu, C.; Yong, X.; Yang, X. Y.; Yu, J. K.; Lu, S. Y.; Bai, F. Q.; Wang, S. P.; Wang, K.; Liu, Z. D.; Feng, B. T.; Hou, X. Y.; Liu, H.; Chen, B. L.; Fang, Q. R.; Zou, B. Pressure engineering toward harvesting the bright deep-blue-light emission in Y-based metal-organic frameworks. *Adv. Funct. Mater.* **2023**, *33*, No. 2300109.
(71) Saraci, F.; Quezada-Novoa, V.; Donnarumma, P. R.; Howarth, A. J. Rare-earth metal-organic frameworks: from structure to applications. *Chem. Soc. Rev.* **2020**, *49*, 7949−7977.
(72) Wang, X.; Jiang, Y.; Tissot, A.; Serre, C. Luminescent sensing platforms based on lanthanide metal-organic frameworks: current strategies and perspectives. *Coord. Chem. Rev.* **2023**, *497*, No. 215454.
(73) Younis, S. A.; Bhardwaj, N.; Bhardwaj, S. K.; Kim, K.-H.; Deep, A. Rare earth metal-organic frameworks (RE-MOFs): synthesis, properties, and biomedical applications. *Coord. Chem. Rev.* **2021**, *429*, No. 213620.
(74) Neese, F. The ORCA program system. *Wiley Interdiscip. Rev.: Comput. Mol. Sci.* **2012**, *2*, 73−78, DOI: 10.1002/wcms.81.
(75) Neese, F.; Wennmohs, F.; Becker, U.; Riplinger, C. The ORCA quantum chemistry program package. *J. Chem. Phys.* **2020**, *152*, No. 224108.
(76) Neese, F. Software update: The ORCA program system-Version 5.0. *Wiley Interdiscip. Rev.: Comput. Mol. Sci.* **2022**, *12*, No. e1606, DOI: 10.1002/wcms.1606.